Published in final edited form as:
Neuroscience. 2009 September 29; 163(1): 329–338. doi:10.1016/j.neuroscience.2009.06.006.

SEX DIFFERENCES IN THE SUBCELLULAR DISTRIBUTION OF AT_1 RECEPTORS AND NADPH OXIDASE SUBUNITS IN THE DENDRITES OF C1 NEURONS IN THE RAT ROSTRAL VENTROLATERAL MEDULLA

Joseph P. Pierce[1], **Justin Kievits**[1], **Bradley Graustein**[1], **Robert C. Speth**[3], **Costantino Iadecola**[1], and **Teresa A. Milner**[1,2]

[1] Division of Neurobiology, Department of Neurology and Neuroscience, Weill Cornell Medical College, 407 East 61st Street, New York, NY 10065

[2] Harold and Margaret Milliken Hatch Laboratory of Neuroendocrinology, The Rockefeller University, 1230 York Avenue, New York, NY 10065

[3] University of Mississippi School of Pharmacy, Department of Pharmacology, University of Mississippi, University, MS 38677

Abstract

The rostral ventrolateral medulla (RVLM), a region critical for the tonic and reflex control of arterial pressure, contains a group of adrenergic (C1) neurons that project to the spinal cord and directly modulate pre-ganglionic sympathetic neurons. Epidemiological data suggests that there are gender differences in the regulation of blood pressure. One factor that could be involved is angiotensin II signaling and the associated production of reactive oxygen species (ROS) by NADPH oxidase, which is emerging as an important molecular substrate for central autonomic regulation and dysregulation. In this study dual electron microscopic immunolabeling was used to examine the subcellular distribution of the angiotensin type 1 (AT_1) receptor and two NADPH oxidase subunits (p47 and p22) in C1 dendritic processes, in tissue from male, proestrus (high estrogen) and diestrus (low estrogen) female rats. Female dendrites displayed significantly more AT_1 labeling and significantly less p47 labeling than males. While elevations in AT1 labeling primarily resulted from higher levels of receptor on the plasma membrane, p47 labeling was reduced both on the plasma membrane and in cytoplasm. Across the estrous cycle, proestrus females displayed significantly higher levels of AT_1 labeling than diestrus females, which resulted exclusively from plasma membrane density differences. In contrast, p47 labeling did not change across the estrous cycle, indicating that ROS production might reflect AT_1 receptor membrane density. No significant differences in p22 labeling were observed. These findings demonstrate that both sex and hormonal levels can selectively affect the expression and subcellular distribution of components of the angiotensin II signaling pathway within C1 RVLM neurons. Such effects could reflect differences in the capacity for ROS production, potentially influencing short term excitability and long term gene expression in a cell group which is critically involved in blood pressure regulation, potentially contributing to gender differences in the risk of cardiovascular disease.

*Address correspondence to: Drs. Joseph P. Pierce, Division of Neurobiology, Weill Cornell Medical College, 407 East 61st Street, New York, NY 10065, Phone: (646) 962-8256, e-mail: jppierc@med.cornell.edu.

Keywords

C1 neurons; bulbospinal neurons; electron microscopy; NADPH oxidase; angiotensin; reactive oxygen species

Accumulating epidemiological data indicates that gender is a primary determinant in predicting the chance of developing a cardiovascular disease, such as hypertension (Reckelhoff, 2001, Grady et al., 2002). Women under the age of 45 die much less frequently from cardiovascular disorders than men (Albert et al., 1996). After menopause this pattern is reversed (Sourander et al., 1998). Animal models of hypertension display comparable sex-associated differences, with blood pressure increases occurring later, and in a less pronounced manner, in females (Ouchi et al., 1987, Xue et al., 2007, Girouard et al., 2008).

A restricted group of central nervous system pathways is thought to be integrally involved in the development and maintenance of hypertension (Korner, 2007). A key component of these pathways is the rostral ventrolateral medulla (RVLM), which contains tonically active bulbospinal neurons, most of which express tyrosine hydroxylase (TH) (the C1 cell group (Phillips et al., 2001)). These bulbospinal neurons are the dominant source of excitatory drive to sympathetic efferent projections in the spinal cord, and are thus vital to the maintenance of sympathetic vasomotor tone (Aicher et al., 2000, Card et al., 2006, Guyenet, 2006). Although anti-dopamine-β-hydroxylase-saporin studies have shown that the C1 cell group is not essential for the RVLM-mediated maintenance of resting sympathetic vasomotor tone, they are a primary contributor, and play a substantial role in cardiovascular regulation through involvement in several sympathoexcitatory reflexes (Schreihofer et al., 2000, Madden and Sved, 2003). Since sustained increases in sympathoexcitation play a role in hypertension, RVLM bulbospinal neurons represent a point at which sex differences could affect cardiovascular vulnerability.

The renin-angiotensin system is present in the central nervous system, and is directly involved in both the central regulation of arterial pressure and in mechanisms of hypertension (Peterson et al., 2006). Both sympathetic nerve activity and blood pressure increase following the injection of angiotensin II (AngII) into the RVLM (Averill et al., 1994, Hirooka et al., 1997). These effects are blocked by antagonists of angiotensin type 1 (AT_1) receptors, which are present in the RVLM (Dampney, 1994, Allen et al., 2006, Chan et al., 2007). Reactive oxygen species (ROS) have emerged as key mediators of the central effects of AngII (Zimmerman et al., 2004, Sun et al., 2005). AngII binding to AT_1 receptors induces the phosphorylation of p47, a cytoplasmic subunit of NADPH oxidase, which then translocates to the plasma membrane (Infanger et al., 2006). This translocation is an essential step in the assembly of the NADPH oxidase complex, and the initiation of ROS production (Sumimoto et al., 2005). Intracerebroventricular infusion of AngII increases ROS production in the RVLM (Gao et al., 2005), and the associated increases in sympathetic activity can be reduced by NADPH oxidase inhibition (Chan et al., 2005). Therefore, sex differences in AT_1 signaling and/or NADPH oxidase activity within the RVLM could be associated with differences in the likelihood of hypertension. Determining the subcellular distribution of both the AT_1 receptor and components of NADPH oxidase is critical to understanding the functional state of this signaling pathway. Like other G protein-coupled receptors, the AT_1 receptor can undergo agonist-induced desensitization and internalization (Morinelli et al., 2007). Thus at any given point in time, two distinct populations of AT_1 receptor exist: plasma membrane receptors, which are available for agonist binding, and an internalized pool. The precise subcellular location of NADPH oxidase also determines the effect of ROS production (Wolin, 2004, Ushio-Fukai, 2006), since ROS are both diffusable and short-lived. Transmembrane components of NADPH oxidase, such as p22 or Nox2, are targeted to specific microdomains of the plasma membrane,

or endomembranes, where they can be spatially coupled to oxidant-sensitive proteins. Additionally, as described, p47 translocates between cytoplasmic and membrane-associated positions, its location reflecting the extent of NADPH oxidase assembly and ROS production (Sumimoto et al., 2005). Thus, experimental approaches that determine overall levels of AT_1 or NADPH oxidase subunit protein expression in the RVLM, or C1 neurons, cannot sufficiently elucidate the function of these signaling pathways. An examination of the subcellular distribution of the AT_1 receptor and associated NADPH oxidase subunits within the dendrites of C1 neurons is needed to address these issues, which requires the use of electron microscopic (EM) immunohistochemical techniques.

This study therefore employed preembedding dual EM immunolabeling to examine whether there are differences in the subcellular pattern of labeling of the AT_1 receptor, and p22 and p47 NADPH oxidase subunits, in RVLM C1 neurons, identified by TH immunoreactivity. Tissue from adult male, proestrus (high estrogen) and diestrus (low estrogen) female rats was processed in parallel to allow an analysis of both sex differences, and changes across the estrous cycle. The findings of this study reveal that both AT_1 and p47 immunolabeling of C1 dendrites differs significantly between males and females, indicating that gender-related distinctions in AngII signaling might exist in this cell population. Additionally, the density of AT_1 labeling of the plasma membrane varied with the estrous cycle, suggesting that AngII sensitivity might also vary in a comparable manner.

EXPERIMENTAL PROCEDURES

Animals

Adult (4 month, 200–300 g) male (n = 4) and female (n = 7) Sprague–Dawley rats were purchased from Charles River Laboratories (Wilmington, MA). The estrous stage of females was determined using vaginal smear cytology (Turner and Bagnara, 1971) after at least two full cycles (diestrus, n = 4; proestrus, n = 3). Rats were housed with 12:12-h light/dark cycles (lights on 0600–1800). All procedures were carried out in accordance with the NIH Guidelines and were approved by the Institutional Animal Care and Use Committee at Weill Cornell Medical College.

Antisera

The AT_1 receptor was labeled using an affinity purified rabbit antiserum (#92578) raised against the C terminal portion (amino acids 341–355) of the rat AT_{1A} receptor. The antiserum is the same as that used in earlier studies of AT_{1A} receptor distribution (Huang et al., 2003, Glass et al., 2005, Glass et al., 2007), except that it was not purified for separation of the AT_{1A} and AT_{1B} subtypes, and is thus designated as an AT_1 receptor antiserum. The selectivity of this antiserum for AT_1 versus AT_2 receptors has been demonstrated using Chinese hamster ovary cells differentially transfected with the receptors (Huang et al., 2003), and preadsorption tests with the AT_1 peptide have been conducted (Huang et al., 2003). The NADPH oxidase subunits p47 and p22 were visualized using affinity-purified goat antisera (p47, sc-7660; p22, sc-11712) obtained from Santa Cruz Biotechnology (Santa Cruz, CA), and were raised against C terminal portions of peptides of human origin. These antisera show recognition of their respective epitopes using Western blotting and immunoprecipitation (manufacturer's data), and have been both extensively characterized and localized using immunogold labeling techniques and tested through preadsorption (Glass et al., 2006, Glass et al., 2007). C1 neurons were identified using a well characterized monoclonal mouse antibody raised against an epitope within the midportion of the TH amino acid sequence (ImmunoStar, Hudson, WI) (Glass et al., 2001).

Electron Microscopic Immunocytochemistry

All rats were anesthetized with sodium pentobarbital (150 mg/kg i.p.), and sequentially perfused transcardially with a saline-heparin solution, 3.75% acrolein and 2% paraformaldehyde (PF) in 0.1 M phosphate buffer (PB) and 2% PF in PB. Brains were then blocked and postfixed in 2% PF in PB. Vibratome sections (40 μm) through the entire extent of the RVLM were cut into cold PB, transferred to a storage solution (30% sucrose and 10% ethylene glycol in 0.1 M PB) and stored at −25 °C. Random systematic series of sections (1:6) through the RVLM of each animal were then processed in parallel to immunoperoxidase (ImP) label TH and immunogold (ImG) label either the AT_1 receptor, p47 subunit, or p22 subunit. For each antibody pairing, all tissue sections were processed simultaneously, so that they would be exposed to exactly the same concentrations for exactly the same periods of time.

Following sodium borohydride and freeze-thaw treatments (for procedural details see (Pierce et al., 2005)), and incubation in a 0.5% bovine serum albumin (BSA) solution, free floating tissue sections were placed in an antibody solution containing either the AT_1 receptor antibody (1:200), the p47 antibody (1:100), or the p22 antibody (1:500) in 0.1% BSA/tris saline (TS), for 48 hr at RT. At 24 hr, TH antibody (1:20,000) was added to the primary antibody diluent. Processes containing TH were then ImP-labeled with the avidin-biotin-peroxidase complex method (Hsu et al., 1981), using the following incubations separated by rinses: (a) a 1:400 dilution of horse anti-mouse biotinylated-IgG in 0.1% BSA/TS, 30 min (Jackson Immunoresearch, West Grove, PA), (b) a 1:100 dilution of avidin-biotin-peroxidase complex in 0.05% BSA/TS (Vectastain Elite Kit, Vector Laboratories, Burlingame, CA), 30 min, (c) 0.022% 3,3′-diaminobenzidine and 0.003% H_2O_2 in TS, 8 min, and (d) a PB wash, 10 min. Sections were further processed to ImG-label AT_1, p47 or p22 through: (a) PB saline (PBS, 0.9% NaCl in 0.01 M PB, ph 7.4), 10 min, (b) blocking buffer (0.8% BSA and 0.1% gelatin in PBS), 10 min, (c)1 nm gold particle-conjugated goat anti-rabbit, or donkey anti-goat, IgG (Electron Microscopy Sciences Inc., Hatfield, PA) in blocking buffer, 18 hr; (d) blocking buffer, 5 min, (e) PBS rinses and postfixation in 2% glutaraldehyde, 10 min, (f) citrate buffer (0.2 M, ph 7.4), 10 min, (g) silver intensification using an IntenSE-M Kit (Amersham, Arlington Heights, IL), 7 min, and (i) citrate buffer wash, 10 min. Preparation for EM examination involved: (a) PB wash, 5 min, (b) postfixation in 2% osmium, 1 hr, (c) dehydration in a series of graded alcohols and propylene oxide, (d) 1:1 Embed 812 (Electron Microscopy Sciences Inc., Hatfield, PA) and propylene oxide, 12 hr, (e) 100% Embed 812, 2 hrs, (f) flat-embedding between Aclar film (Allied Signal, Pottsville, PA), and (g) polymerization at 60° C, 72 hr. Randomly selected RVLM sections containing C1 TH-labeled neurons from each animal were excised, glued onto blocks, and sectioned on a Leica UCT ultratome. The C1 area of RVLM corresponded to AP = −12.50 to −12.68 from bregma (levels 62–63 of Swanson (Swanson, 1999)). The area selected for analysis was caudal to the facial nucleus, rostral to the A1 region (Ross et al., 1984), ventral to the nucleus ambiguus, and flanked by the inferior olive, spinal trigeminal tract and ventral surface of the medulla. Thin sections (70 nm) were collected on thin Bar copper mesh grids (Electron Microscopy Sciences Inc., Hatfield, PA), and counterstained with uranyl acetate and Reynold's lead citrate prior to examination on a Tecnai electron microscope (FEI Company, Hillsboro, OR).

Electron Microscopic Sampling and Analysis

Randomly selected thin sections from near the surface of each block (which contained a plastic/tissue interface, indicating the surface of the Vibratome tissue section) were examined. To control for the effect of penetration, only tissue fields adjacent to the plastic/tissue interface were analyzed (Auchus and Pickel, 1992). This limited analysis to the most superficial portions of the tissue (0.1–1 μm from the surface) that displayed the most robust labeling, and ensured that a comparable tissue depth would be examined for all animals. Every TH ImP-labeled dendritic profile (identified by being postsynaptic to presynaptic terminals (Peters et al.,

1991)) in a randomly selected series of plastic/tissue interface adjacent grid square fields (2916 μm^2 per grid square field) was examined, and digital images were captured with an AMT Advantage HR/HR-B CCD Camera System (Advanced Microscopy Techniques, Danvers, MA), at magnifications from 9,000x to 23,000x). TH ImP-labeled dendritic profiles that did not display any ImG-labeling were also included in the analysis, to generate the most accurate measure of the overall density of ImG-labeling within TH-labeled dendrites. For each antibody pairing, from 9 to 27 grid squares per animal were examined (total areas examined: TH-AT_1 tissue, 282,900 μm^2; TH-p47 tissue, 392,500 μm^2; TH-p22 tissue, 250,800 μm^2), yielding 42 to 127 TH ImP-labeled dendritic profiles (total profile number: TH-AT_1 tissue, 836; TH-p47 tissue, 735; TH-p22 tissue, 617).

Analysis of the Distribution Pattern of Immunogold Particles

Each TH ImP-labeled dendritic profile was analyzed to determine: 1) the length of the profile perimeter in μms, 2) the cross-sectional area of the profile in μm^2s, 3) the number of ImG particles that were located within the profile, and 4) the diameter of the profile in μms. ImG particles within the profile were also subdivided into those that directly contacted the plasma membrane, and those that did not. Measurements were made on digital images using Microcomputer Imaging Device software (MCID; Imaging Research, St. Catharines, Ontario, Canada). These values were used to determine the density of ImG particle labeling on the plasma membrane (ImP/μm) and within the cytoplasm (ImG/μm^2). In addition, for each antibody pairing run, 100 ImG particles were randomly selected and analyzed to determine their size (in terms of cross-sectional area, μm^2) and circularity (the ratio of perimeter to area, normalized so that a circle of the same area will have a roundness of 1.0). ImG particles were traced, and the tracing was scanned, thresholded, and imported into ImageJ, where particle analysis was used to determine these measurements. Since every ImG particle labeling a TH-positive dendritic profile was included in the analysis, the validity of the approach rests on the extremely low levels of non-specific, background ImG labeling produced by preembedding labeling techniques. With omission of the primary antibody, and using the same secondary antibody dilutions employed in this study, non-specific labeling has been estimated to represent 3% of all preembedding ImG labeling (Wang et al., 2003).

Determining Whether Immunogold Particles are Distributed Non-Randomly

Examination of the distribution of ImG particles in relation to a specific subcellular structure, like the plasma membrane, rests on the assumption that the ImG particles are distributed selectively, in a non-random manner. This assumption can be directly tested by determining the number of ImG particles that would be observed in contact with the membrane, on average, if they were distributed randomly within the profile, and statistically comparing this estimate with actual experimental values. The probability that an ImG particle would randomly contact the plasma membrane of a profile depends on several factors: the membrane length, the profile area, and the average ImG particle size. Assuming that ImG particles are circular, one can define a ring-shaped region (‘membrane area’) around the inside of the profile membrane, with the thickness of the ring equal to the average ImG particle radius. If, on average, the center of an ImG particle falls within this area, it will contact the membrane- if it falls outside this area (more centrally within the profile), it will not (Fig. 1). Then, the percent of ImG particles that would contact the membrane if they were randomly distributed within the profile is equal to the fraction of the total profile area occupied by the membrane area, and can be calculated with the equation: % random contact = [(profile perimeter × average immunogold particle radius)/ profile area] × 100. Since all of the primary antibodies used in this study were raised against C terminus epitopes of proteins, which are positioned on the cytoplasmic side of the plasma membrane, only ImG particles contacting the membrane from this side were counted.

Statistical Analysis

The statistical significance between groups was analyzed using Student's *t* tests. To test for sex differences, male and female (pooled proestrus and diestrus females) values were compared. To test for differences along the estrous cycle, proestrus and diestrus female values were compared. *P* values < 0.05 were considered significant. Values were reported as mean ± SEM.

Figure Preparation

Light and electron micrographs were imported into Adobe Photoshop CS3 (Adobe Systems Inc. (San Jose, CA) as greyscale images, and the levels and sharpness of each image were adjusted to provide proper contrast and detail.

RESULTS

Light and Electron Microscopic Labeling

As has been reported in previous light microscopic studies (Ross et al., 1984, Wang et al., 2006b) the C1 area of the RVLM of male and female rats contained numerous TH-labeled neurons with long thin dendrites (Fig. 2). These dendrites ramified extensively within the region, forming a network of processes that at times could be observed closely associated with blood vessels. At the ultrastructural level, TH-ImP labeled dendritic processes were also clearly visible, and frequently displayed either AT_1, p47 or p22 ImG labeling (Fig. 3). AT_1 ImG labeling was also observed in glial processes (Fig. 3d) and non-TH-positive dendrites, and less frequently in presynaptic processes (Fig. 3a) and vascular endothelial cells. Both p47 and p22 ImG labeling were often observed in non-TH-positive dendrites, glial processes (Figs. 3e, 3h), presynaptic processes (Fig. 3h) and endothelial cells.

AT_1, p47 and p22 ImG Particles Display Distinct, Non-Random Distribution Patterns within C1 Dendrites

In this study, the average circularity values for ImG particles was 0.82 ± 0.01 (for p47), 0.85 ± 0.01 (for p22) and 0.81 ± 0.01 (for AT_1), suggesting that the assumption of circularity is reasonable. If ImG particles were randomly distributed within the measured profiles, it is estimated that 8.0 ± 0.9% (for p47), 10.0 ± 0.5% (for p22) and 17.2 ± 0.8% (for AT_1) of ImG particles would be observed contacting the plasma membrane. These values are all significantly lower that the observed values (% M (membrane) ImG particles: 21 ± 2% (for p47, p = 0.01, n = 735), 20 ± 2% (for p22, p = 0.01, n = 617) and 33 ± 4% (for AT_1, p = 0.005, n = 836), using paired t-tests), indicating that ImG particles were selectively distributed along the membrane.

Thus, two distinct populations of ImG particles exist: membrane-associated particles (measured in terms of ImG/μm profile perimeter), and internal particles (measured in terms of ImG/μm^2 profile area). This distinction has different functional implications for p47, versus AT_1 and p22. P47 is a cytoplasmic protein that translocates to the membrane in association with the assembly of the NADPH oxidase complex (Infanger et al., 2006). The AT_1 receptor and p22 subunit are both transmembrane proteins, so internal 'cytoplasmic' labeling presumably represents the labeling of endomembranes, which are quite delicate and often damaged during tissue processing (Pierce et al., 2000).

C1 Dendrites in Females have More AT_1 ImG Labeling and Less p47 Labeling than Males

To determine if there were significant differences in the overall level of AT_1 ImG labeling of TH ImP dendritic profiles, the total number of ImG particles per profile was first examined. Females displayed significantly more AT_1 ImG labeling than males (0.59 ± 0.06 ImG/profile

versus 0.40 ± 0.05 ImG/profile, p = 0.01, n = 836) (Fig. 4). This primarily resulted from a striking difference in membrane-associated labeling: the density of AT_1 ImG particles on the dendrites of females was 2.1x that of males (females: 0.034 ± 0.005 ImG/μm, males: 0.016 ± 0.004 ImG/μm, p = 0.01). The density of ImG particles within the cytoplasm (females: 0.18 ± 0.03 ImG/μm^2, males: 0.12 ± 0.03 ImG/μm^2) was not significantly different (p > 0.05), and the relative distribution on AT_1 ImG particles also did not differ significantly: 36 ± 4% were on the membrane in females, versus 30 ± 5% in males (p > 0.05).

Compared to AT_1, p47 ImG labeling exhibited an inverse pattern, with females displaying roughly half as much labeling as males (1.9 ± 0.2 ImG/profile versus 3.7 ± 0.6 ImG/profile, p = 0.0001, n = 735) (Fig. 4). In this instance, comparably lower densities of labeling were observed both on the membrane (females: 0.059 ± 0.006 ImG/μm, males: 0.14 ± 0.02 ImG/μm, p = 0.0001) and in the cytoplasm (females: 0.57 ± 0.04 ImG/μm^2, males: 1.1 ± 0.1 ImG/μm^2, p = 0.0001). The relative distribution was maintained: 23 ± 3% were on the membrane in females versus 19 ± 2% in males. P22 ImG labeling did not differ significantly between males and females in terms of any of the variables measured (Fig. 4).

Proestrus is Associated with Increases in AT_1 ImG Labeling that are Totally Restricted to the Dendritic Surface

Data obtained from female rats was then subdivided in terms of the estrous cycle stage of the animal, to determine if the pattern of AT_1 and NADPH oxidase subunit labeling changed in parallel with hormonal fluctuations. Significantly higher levels of AT_1 ImG labeling were observed during proestrus (high estrogen) in comparison to diestrus (low estrogen) (0.7 ± 0.1 ImG/profile versus 0.44 ± 0.07 ImG/profile, p = 0.01, n = 475) (Fig. 4). This resulted entirely from a dramatic shift in the density of AT_1 ImG labeling on the membrane, with proestrus values being 2.2x those observed at diestrus (proestrus: 0.047 ± 0.008 ImG/μm, diestrus: 0.021 ± 0.006 ImG/μm, p = 0.007). In contrast, the density of labeling within the cytoplasm was not altered (proestrus: 0.18 ± 0.03 ImG/μm^2, diestrus: 0.17 ± 0.06 ImG/μm^2). Therefore, a significant redistribution of AT_1 ImG labeling occurred across the estrous cycle: during proestrus 45 ± 5% of the particles were associated with the membrane, while during diestrus only 25 ± 5% were associated with the membrane (p = 0.005). In contrast, neither the density nor distribution of either p47 or p22 ImG particles changed across the cycle (Fig. 4).

DISCUSSION

These findings demonstrate that both sex- and estrous cycle-related differences exist in the quantity and pattern of AT_1 and p47 immunolabeling of TH-positive dendrites in RVLM C1 neurons in normal adult rats. First, adult females displayed higher overall levels of AT_1 ImG labeling than males. Previous findings indicate that similar elevations in the overall level of AT_1 immunolabeling can be observed in TH-positive RVLM neurons in juvenile (postnatal day 23) and ovariectomized adult females versus males, indicating that this sex difference is present in the prepubertal animal, and persists into adulthood (Wang et al., 2008). Analysis of the subcellular distibution of AT_1 ImG labeling in the present study established that the elevated levels of labeling in females primarily resulted from a significantly denser concentration of labeling on the plasma membrane, where the receptor is accessible to ligand binding. This suggests that C1 neurons could have a greater sensitivity to extracellular AngII in females versus males.

In contrast, a significantly lower level of p47 ImG labeling was observed in adult females. This parallels previous observations in juvenile rats (Wang et al., 2008), indicating that this feature is also present at an early stage, and persists into adulthood. In the current study, significant reductions in p47 ImG labeling were seen both on the membrane, and in the cytoplasm. Since the translocation of p47 from the cytoplasm to a membrane-associated position occurs during

the assembly of the NADPH oxidase complex, and is necessary for ROS production (Sumimoto et al., 2005), reductions in both membrane-associated and reserve cytoplasmic pools of the p47 subunit presumably reflect diminished ROS production, and a diminished capacity for ROS production.

Additionally, females displayed major alterations in both the density and distribution of AT_1 ImG particles across the estrous cycle. First, significantly more AT_1 immunolabeling was present during proestrus, when estrogen levels are highest, compared to diestrus. This parallels previous observations indicating that estrogen treatment of ovariectomized adult females produces significantly higher overall levels of AT_1 labeling than vehicle treated controls (Wang et al., 2008). Thus, the level of AT_1 labeling fluctuated across the estrous cycle. These changes were almost exclusively restricted to the dendritic surface, as evidenced by a parallel shift in the relative distribution of ImG labeling, with a much greater proportion of ImG particles on the surface during proestrus. The cytoplasmic density of AT_1 ImG labeling remained virtually unchanged across the cycle, implying that reserve pools of receptor were maintained during times when there was greater targeting of receptor to the membrane. ImG labeling for both the p47 and p22 NADPH oxidase subunits also remained unchanged across the estrous cycle, suggested that, if the components of the NADPH oxidase complex were present in sufficient quantity to fully support AngII-induced ROS production, the shifts in plasma membrane AT_1 ImG labeling would reflect a fluctuating capacity for ROS production across the cycle.

Both AT_1 receptors and NADPH oxidase, as a generator of ROS, are critically involved in central hypertension mechanisms (Wang et al., 2004, Gao et al., 2005, Sun et al., 2005, Zimmerman et al., 2005, Wang et al., 2006a). The observation that there are significant sex-related differences in the subcellular distribution of these components within RVLM C1 neurons, a principal source of excitatory drive to sympathetic efferent projections in the spinal cord (Aicher et al., 2000, Card et al., 2006, Guyenet, 2006), suggests that this cell group could be central to the mediation of differences in blood pressure regulation. In various animal models of hypertension, including AngII infusion (Xue et al., 2005, Girouard et al., 2008), deoxycorticosterone-salt (Ouchi et al., 1987) and spontaneously hypertensive rats (Reckelhoff, 2001), males display greater elevations of blood pressure than females, a pattern that parallels gender differences in clinical studies of subjects under 45 (Albert et al., 1996). In this context, the current AT_1 receptor findings could appear counterintuitive, since greater concentrations, particularly on the plasma membrane, would suggest that female C1 neurons were more sensitive to AngII. However, the parallel reductions in p47 levels, both on the membrane and in the cytoplasm of female C1 neurons, may represent a compensatory adjustment, in both ROS production, and the capacity for ROS production. Data obtained from juveniles, where a pattern of labeling comparable to adults is observed (Wang et al., 2008), supports this contention: AngII induces similar levels of ROS production in C1 neurons isolated from males and females. Such differences could also reflect a greater role for non-ROS-dependent AT_1 receptor-mediated signaling, such as effects on phospholipase pathways and prostaglandin metabolism (Berry et al., 2001), in females.

Such balanced shifts in AT_1 signaling components underscores the apparent complexity of sex-associated differences within this cell population. Juvenile C1 neurons isolated from females also display significantly larger AngII-induced, ROS-dependent L-type Ca^{2+} currents than males (Wang et al., 2008), which appears attributable to differences in the number and/or sensitivity of L-type Ca^{2+} channels, since comparable results can be obtained when AT_1 signaling is blocked and an L-type Ca^{2+} channel activator is applied. Sex-differences in these components could, in addition to influencing neuronal excitability, also have long-term sustained effects, since AT_1 receptor activation (Sumners et al., 2002), ROS production (Shi and Gibson, 2007), and L-type Ca^{2+} activation (Lipscombe et al., 2004) are all known to

regulate gene expression. Future studies will be required to determine if these factors contribute to sex differences in hypertension susceptibility.

As mentioned, in females some of these factors are also influenced by the estrous cycle. Variations in the density of AT_1 receptors on the plasma membrane of C1 neurons across the cycle could reflect a fluctuating capacity for ROS production, which would be positively correlated with estrogen levels. Estrogens are thought to exert a protective effect in relation to cardiovascular disorders, such as stroke, both centrally (Yang et al., 2005) and in the vasculature (Kim et al., 2008), and can directly influence the function of central autonomic nuclei in females. Injection of estrogen into the RVLM exerts a sympathoinhibitory effect (Saleh et al., 2000), lowering mean arterial pressure, and the application of 17β-estradiol to isolated RVLM bulbospinal neurons decreases L-type Ca^{2+} currents (Wang et al., 2006b). Such effects could mask an underlying, increased sensitivity to AngII during periods of high estrogen levels, potentially as the result of a compensatory overexpression, or increased membrane targeting of AT_1 receptors. Estrogen and AngII can act in opposition to modulate processes, such as the regulation of water intake (Kisley et al., 1999). The increased sensitivity might only become apparent when AngII levels were high enough to override the concurrent effects of estrogen.

In summary, these findings reveal the existence of novel, potentially interdependent sex-and hormone-related differences in the expression and distribution of AT_1 signaling components in the C1 RVLM cell group. These differences could directly affect both short term excitability and long term gene expression in these cells, which are critically involved in the maintenance of sympathoexcitatory drive and blood pressure regulation, potentially contributing to gender differences in the risk of cardiovascular disease.

Acknowledgments

Supported by HL18974

Abbreviations

AngII
: angiotensin II

AT_1
: angiotensin type 1

BSA
: bovine serum albumin

EM
: electron microscopic

ImG
: immunogold

ImP
: immunoperoxidase

M
: membrane

NADPH
: nicotinamide adenine dinucleotide phosphate

PB
phosphate buffer

PBS
PB saline

PF
paraformaldehyde

ROS
reactive oxygen species

RVLM
rostral ventrolateral medulla

TH
tyrosine hydroxylase

TS
tris saline

BIBLIOGRAPHY

Aicher SA, Milner TA, Pickel VM, Reis DJ. Anatomical substrates for baroreflex sympathoinhibition in the rat. Brain Res Bull 2000;51:107–110. [PubMed: 10709955]

Albert CM, McGovern BA, Newell JB, Ruskin JN. Sex differences in cardiac arrest survivors. Circulation 1996;93:1170–1176. [PubMed: 8653838]

Allen AM, Dosanjh JK, Erac M, Dassanayake S, Hannan RD, Thomas WG. Expression of constitutively active angiotensin receptors in the rostral ventrolateral medulla increases blood pressure. Hypertension 2006;47:1054–1061. [PubMed: 16618838]

Auchus AP, Pickel VM. Quantitative light microscopic demonstration of increased pallidal and striatal Met^5-enkephalin like immunoreactivity in rats following chronic haloperidol but not with clozapine. Exp Neurol 1992;117:17–27. [PubMed: 1618284]

Averill DB, Tsuchihashi T, Khosla MC, Ferrario CM. Losartan, nonpeptide angiotensin II-type 1 (AT1) receptor antagonist, attenuates pressor and sympathoexcitatory responses evoked by angiotensin II and L-glutamate in rostral ventrolateral medulla. Brain Res 1994;665:245–252. [PubMed: 7895060]

Berry C, Touyz R, Dominiczak AF, Webb RC, Johns DG. Angiotensin receptors: signaling, vascular pathophysiology, and interactions with ceramide. Am J Physiol Heart Circ Physiol 2001;281:H2337–2365. [PubMed: 11709400]

Card JP, Sved JC, Craig B, Raizada M, Vazquez J, Sved AF. Efferent projections of rat rostroventrolateral medulla C1 catecholamine neurons: Implications for the central control of cardiovascular regulation. J Comp Neurol 2006;499:840–859. [PubMed: 17048222]

Chan SH, Hsu KS, Huang CC, Wang LL, Ou CC, Chan JY. NADPH oxidase-derived superoxide anion mediates angiotensin II-induced pressor effect via activation of p38 mitogen-activated protein kinase in the rostral ventrolateral medulla. Circ Res 2005;97:772–780. [PubMed: 16151022]

Chan SH, Wang LL, Tseng HL, Chan JY. Upregulation of AT1 receptor gene on activation of protein kinase Cbeta/nicotinamide adenine dinucleotide diphosphate oxidase/ERK1/2/c-fos signaling cascade mediates long-term pressor effect of angiotensin II in rostral ventrolateral medulla. Journal of hypertension 2007;25:1845–1861. [PubMed: 17762649]

Dampney RA. Functional organization of central pathways regulating the cardiovascular system. Physiol Rev 1994;74:323–364. [PubMed: 8171117]

Gao L, Wang W, Li YL, Schultz HD, Liu D, Cornish KG, Zucker IH. Sympathoexcitation by central ANG II: roles for AT1 receptor upregulation and NAD(P H oxidase in RVLM. Am J Physiol Heart Circ Physiol 2005;288:H2271–2279. [PubMed: 15637113]

Girouard H, Lessard A, Capone C, Milner TM, Iadecola C. The neurovascular dysfunction induced by angiotensin II in the mouse neocortex is sexually dimorphic. Am J Physiol (Heart and Circ Physiol) 2008;294:H156–163. [PubMed: 17982007]

Glass MJ, Chan J, Frys KA, Oselkin M, Tarsitano MJ, Iadecola C, Pickel VM. Changes in the subcellular distribution of NADPH oxidase subunit p47phox in dendrites of rat dorsomedial nucleus tractus solitarius neurons in response to chronic administration of hypertensive agents. Exp Neurol 2007;205:383–395. [PubMed: 17418121]

Glass MJ, Huang J, Aicher SA, Milner TA, Pickel VM. Subcellular localization of alpha-2A-adrenergic receptors in the rat medial nucleus tractus solitarius: regional targeting and relationship with catecholamine neurons. J Comp Neurol 2001;433:193–207. [PubMed: 11283959]

Glass MJ, Huang J, Oselkin M, Tarsitano MJ, Wang G, Iadecola C, Pickel VM. Subcellular localization of nicotinamide adenine dinucleotide phosphate oxidase subunits in neurons and astroglia of the rat medial nucleus tractus solitarius: relationship with tyrosine hydroxylase immunoreactive neurons. Neuroscience 2006;143:547–564. [PubMed: 17027166]

Glass MJ, Huang J, Speth RC, Iadecola C, Pickel VM. Angiotensin II AT-1A receptor immunolabeling in rat medial nucleus tractus solitarius neurons: subcellular targeting and relationships with catecholamines. Neuroscience 2005;130:713–723. [PubMed: 15590154]

Grady D, Herrington D, Bittner V, Blumenthal R, Davidson M, Hlatky M, Hsia J, Hulley S, Herd A, Khan S, Newby LK, Waters D, Vittinghoff E, Wenger N. Cardiovascular disease outcomes during 6.8 years of hormone therapy: Heart and Estrogen/progestin Replacement Study follow-up (HERS II). Jama 2002;288:49–57. [PubMed: 12090862]

Guyenet PG. The sympathetic control of blood pressure. Nat Rev Neurosci 2006;7:335–346. [PubMed: 16760914]

Hirooka Y, Potts PD, Dampney RA. Role of angiotensin II receptor subtypes in mediating the sympathoexcitatory effects of exogenous and endogenous angiotensin peptides in the rostral ventrolateral medulla of the rabbit. Brain Res 1997;772:107–114. [PubMed: 9406962]

Hsu SM, Raine L, Fanger H. Use of avidin-biotin-peroxidase complex (ABC) in immunoperoxidase techniques: a comparison between ABC and unlabeled antibody (PAP) procedures. J Histochem Cytochem 1981;29:557–580.

Huang J, Hara Y, Anrather J, Speth RC, Iadecola C, Pickel VM. Angiotensin II subtype 1A (AT1A) receptors in the rat sensory vagal complex: subcellular localization and association with endogenous angiotensin. Neuroscience 2003;122:21–36. [PubMed: 14596846]

Infanger DW, Sharma RV, Davisson RL. NADPH oxidases of the brain: distribution, regulation, and function. Antioxid Redox Signal 2006;8:1583–1596. [PubMed: 16987013]

Kim KH, Moriarty K, Bender JR. Vascular cell signaling by membrane estrogen receptors. Steroids 2008;73:864–869. [PubMed: 18325557]

Kisley LR, Sakai RR, Ma LY, Fluharty SJ. Ovarian steroid regulation of angiotensin II-induced water intake in the rat. Am J Physiol 1999;276:R90–96. [PubMed: 9887181]

Korner, PI. Essential Hypertension and Its Causes. New York: Oxford University Press; 2007.

Lipscombe D, Helton TD, Xu W. L-type calcium channels: the low down. J Neurophysiol 2004;92:2633–2641. [PubMed: 15486420]

Madden CJ, Sved AF. Cardiovascular regulation after destruction of the C1 cell group of the rostral ventrolateral medulla in rats. Am J Physiol Heart Circ Physiol 2003;285:H2734–2748. [PubMed: 12933337]

Morinelli TA, Raymond JR, Baldys A, Yang Q, Lee MH, Luttrell L, Ullian ME. Identification of a putative nuclear localization sequence within ANG II AT(1A) receptor associated with nuclear activation. American journal of physiology 2007;292:C1398–1408. [PubMed: 17166941]

Ouchi Y, Share L, Crofton JT, Iitake K, Brooks DP. Sex difference in the development of deoxycorticosterone-salt hypertension in the rat. Hypertension 1987;9:172–177. [PubMed: 3818014]

Peters, A.; Palay, SL.; Webster, Hd. The Fine Structure of the Nervous System: the Neurons and Supporting Cells. Philadelphia: W.B. Saunders Co; 1991.

Peterson JR, Sharma RV, Davisson RL. Reactive oxygen species in the neuropathogenesis of hypertension. Curr Hypertens Rep 2006;8:232–241. [PubMed: 17147922]

Phillips JK, Goodchild AK, Dubey R, Sesiashvili E, Takeda M, Chalmers J, Pilowsky PM, Lipski J. Differential expression of catecholamine biosynthetic enzymes in the rat ventrolateral medulla. J Comp Neurol 2001;432:20–34. [PubMed: 11241375]

Pierce JP, Melton J, Punsoni M, McCloskey DP, Scharfman HE. Mossy fibers are the primary source of afferent input to ectopic granule cells that are born after pilocarpine-induced seizures. Exp Neurol 2005;196:316–331. [PubMed: 16342370]

Pierce JP, van Leyen K, McCarthy JB. Translocation machinery for synthesis of integral membrane and secretory proteins in dendritic spines. Nat Neurosci 2000;3:311–313. [PubMed: 10725917]

Reckelhoff JF. Gender differences in the regulation of blood pressure. Hypertension 2001;37:1199–1208. [PubMed: 11358929]

Ross CA, Ruggiero DA, Joh TH, Park DH, Reis DJ. Rostral ventrolateral medulla: selective projections to the thoracic autonomic cell column from the region containing C1 adrenaline neurons. J Comp Neurol 1984;228:168–185. [PubMed: 6480910]

Saleh MC, Connell BJ, Saleh TM. Autonomic and cardiovascular reflex responses to central estrogen injection in ovariectomized female rats. Brain Res 2000;879:105–114. [PubMed: 11011011]

Schreihofer AM, Stornetta RL, Guyenet PG. Regulation of sympathetic tone and arterial pressure by rostral ventrolateral medulla after depletion of C1 cells in rat. J Physiol 2000;529(Pt 1):221–236. [PubMed: 11080264]

Shi Q, Gibson GE. Oxidative stress and transcriptional regulation in Alzheimer disease. Alzheimer disease and associated disorders 2007;21:276–291. [PubMed: 18090434]

Sourander L, Rajala T, Raiha I, Makinen J, Erkkola R, Helenius H. Cardiovascular and cancer morbidity and mortality and sudden cardiac death in postmenopausal women on oestrogen replacement therapy (ERT). Lancet 1998;352:1965–1969. [PubMed: 9872245]

Sumimoto H, Miyano K, Takeya R. Molecular composition and regulation of the Nox family NAD(P)H oxidases. Biochem Biophys Res Commun 2005;338:677–686. [PubMed: 16157295]

Sumners C, Fleegal MA, Zhu M. Angiotensin AT1 receptor signalling pathways in neurons. Clin Exp Pharmacol Physiol 2002;29:483–490. [PubMed: 12010196]

Sun C, Sellers KW, Sumners C, Raizada MK. NAD(P H oxidase inhibition attenuates neuronal chronotropic actions of angiotensin II. Circ Res 2005;96:659–666. [PubMed: 15746442]

Swanson, LW. Brain Maps: Structure of the Rat Brain. New York: Elsevier; 1999.

Turner, CD.; Bagnara, JT. General Endocrinology. Philadelphia: W.B. Saunders; 1971.

Ushio-Fukai M. Localizing NADPH oxidase-derived ROS. Sci STKE 2006:re8. [PubMed: 16926363]

Wang G, Anrather J, Glass MJ, Tarsitano MJ, Zhou P, Frys KA, Pickel VM, Iadecola C. Nox2, Ca2+, and protein kinase C play a role in angiotensin II-induced free radical production in nucleus tractus solitarius. Hypertension 2006a;48:482–489. [PubMed: 16894058]

Wang G, Anrather J, Huang J, Speth RC, Pickel VM, Iadecola C. NADPH oxidase contributes to angiotensin II signaling in the nucleus tractus solitarius. J Neurosci 2004;24:5516–5524. [PubMed: 15201324]

Wang G, Drake CT, Rozenblit M, Zhou P, Alves SE, Herrick SP, Hayashi S, Warrier S, Iadecola C, Milner TA. Evidence that estrogen directly and indirectly modulates C1 adrenergic bulbospinal neurons in the rostral ventrolateral medulla. Brain Res 2006b;1094:163–178. [PubMed: 16696957]

Wang G, Milner TA, Speth RC, Gore AC, Wu D, Iadecola C, Pierce JP. Sex Differences in Angiotensin Signaling in Bulbospinal Neurons in the Rat Rostral Ventrolateral Medulla. Am J Physiol Regul Integr Comp Physiol 2008;295:R1149–1157. [PubMed: 18685065]

Wang H, Cuzon VC, Pickel VM. Postnatal development of mu-opioid receptors in the rat caudate-putamen nucleus parallels asymmetric synapse formation. Neuroscience 2003;118:695–708. [PubMed: 12710977]

Wolin MS. Subcellular localization of Nox-containing oxidases provides unique insight into their role in vascular oxidant signaling. Arteriosclerosis, thrombosis, and vascular biology 2004;24:625–627.

Xue B, Pamidimukkala J, Hay M. Sex differences in the development of angiotensin II-induced hypertension in conscious mice. Am J Physiol Heart Circ Physiol 2005;288:H2177–2184. [PubMed: 15626687]

Xue B, Pamidimukkala J, Lubahn DB, Hay M. Estrogen receptor-alpha mediates estrogen protection from angiotensin II-induced hypertension in conscious female mice. Am J Physiol Heart Circ Physiol 2007;292:H1770–1776. [PubMed: 17142339]

Yang SH, Liu R, Perez EJ, Wang X, Simpkins JW. Estrogens as protectants of the neurovascular unit against ischemic stroke. Current drug targets 2005;4:169–177. [PubMed: 15857302]

Zimmerman MC, Lazartigues E, Sharma RV, Davisson RL. Hypertension caused by angiotensin II infusion involves increased superoxide production in the central nervous system. Circ Res 2004;95:210–216. [PubMed: 15192025]

Zimmerman MC, Sharma RV, Davisson RL. Superoxide mediates angiotensin II-induced influx of extracellular calcium in neural cells. Hypertension 2005;45:717–723. [PubMed: 15699459]

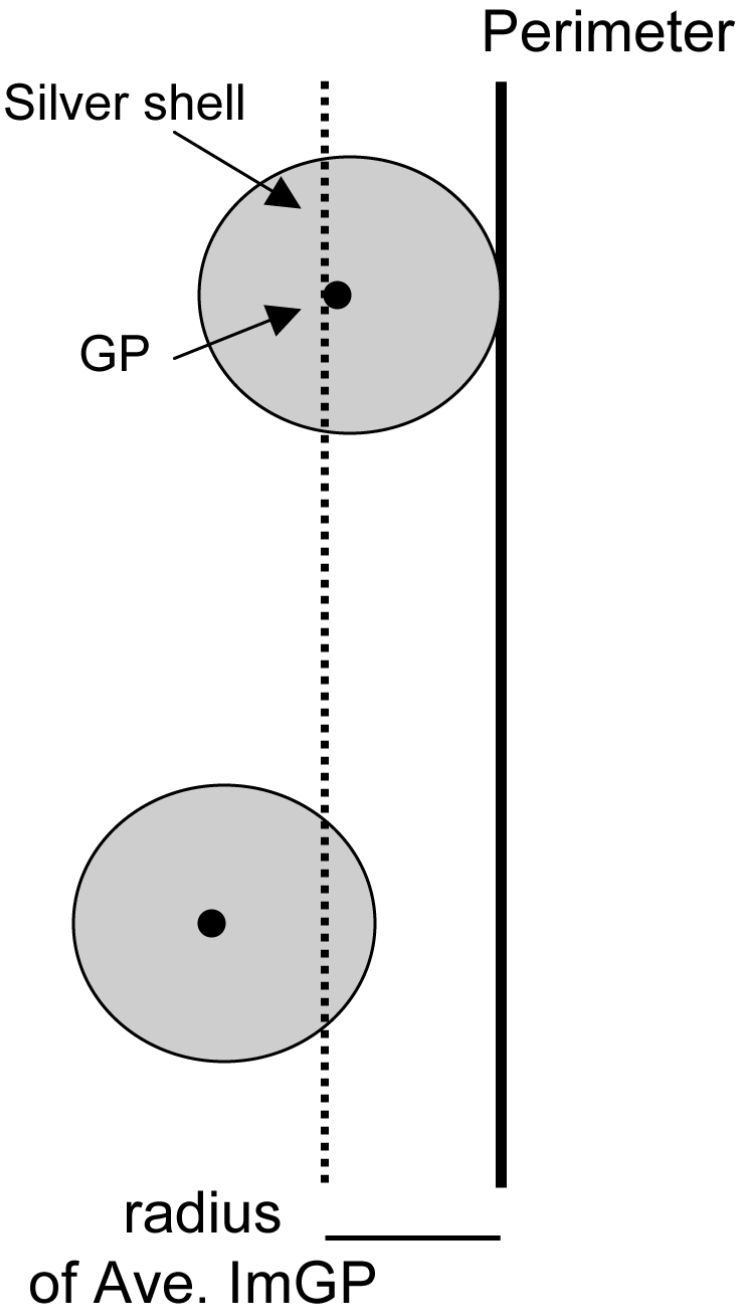

Fig. 1.

Definition of a region around the inside of the perimeter of a profile (‘membrame area’), with a diameter equal to the radius of an average silver-enhanced ImG particle, such that, if on average, the center of an ImG particle falls within this area, it will contact the membrane- if it falls outside this area (more centrally within the profile), it will not. GP, gold particle.

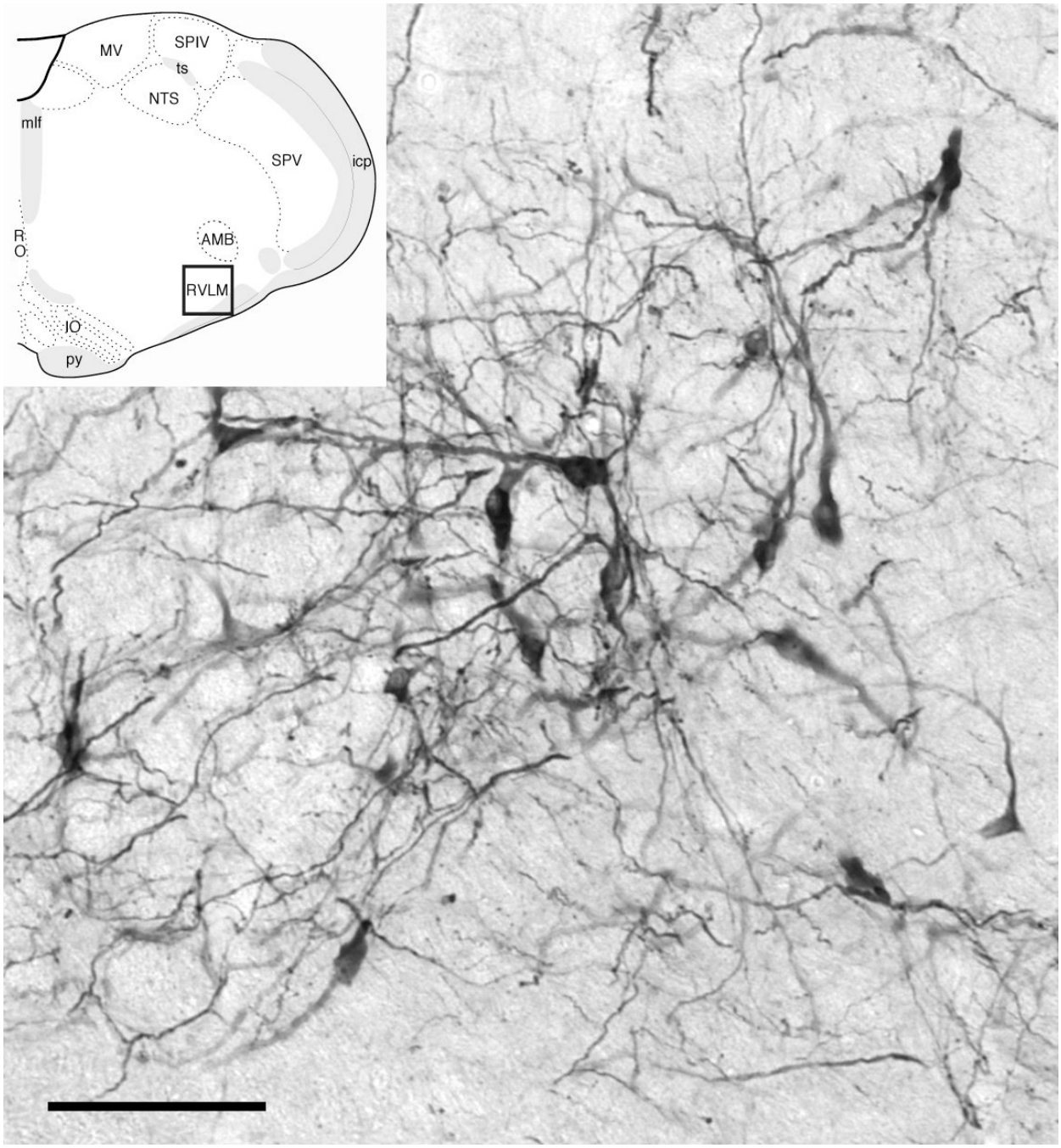

Fig. 2.

Light microscopic analysis of tissue from both males and females revealed that tyrosine hydroxylase (TH)-labeled somata and dendrites produce an extensive network of processes in the C1 region of the RVLM (bar, 100 μm). Insert: Sampled region (black box) (modified from Swanson plate 61 (Swanson, 1999), about 1.2 mm caudal to bregma).

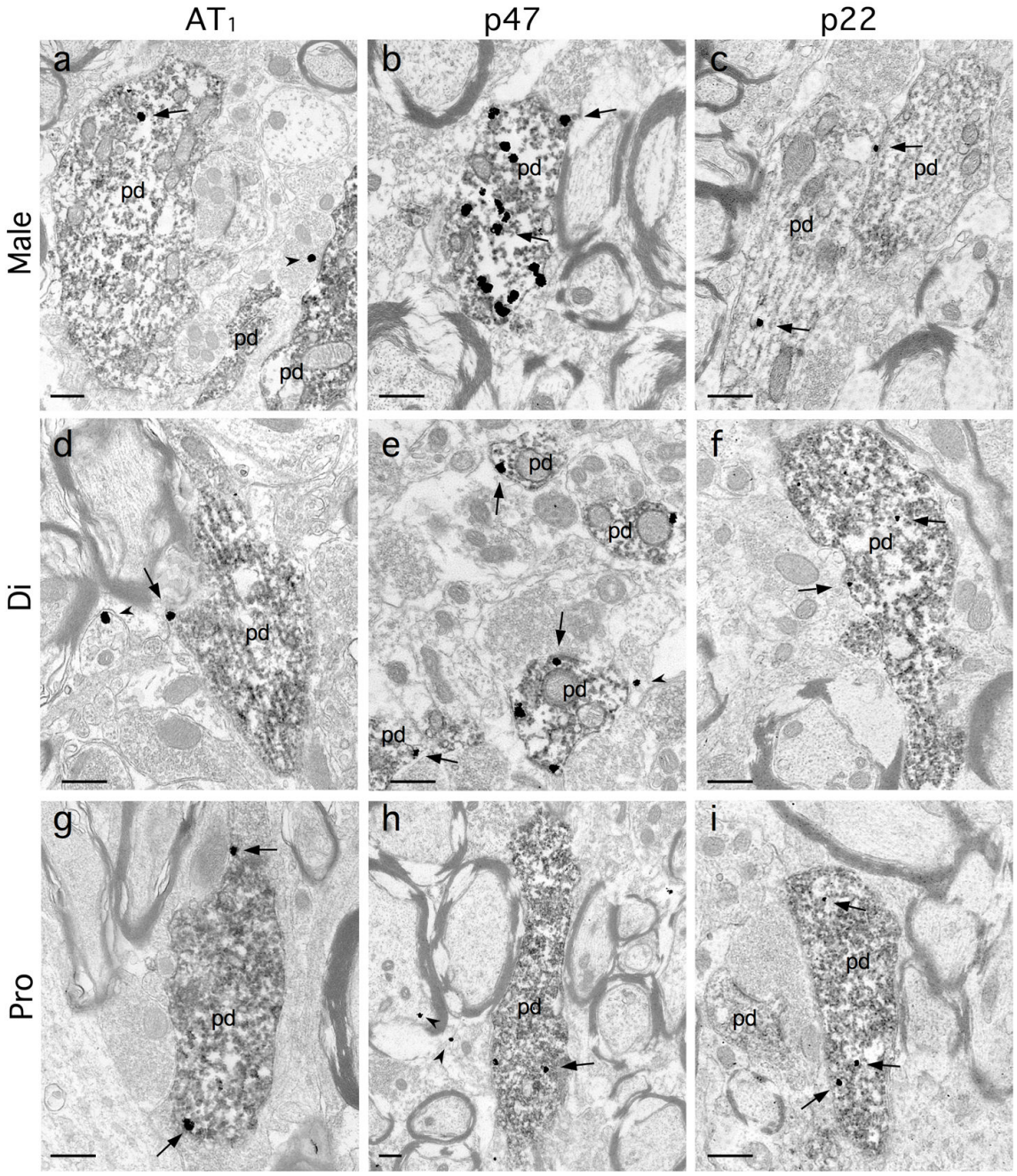

Fig. 3.

At the electron microscopic level, tyrosine hydroxylase (TH)-immunoperoxidase (ImP)-labeled dendrites (pd) were frequently observed in the RVLM of males (a–c), and diestrus (d–f) and proestrus (g–i) females, and often displayed immunogold(ImG)-labeling (arrows) for either the AT_1 receptor (a, d, g), p47 (b, e, h) or p22 (c, f, i). As noted, ImG particles were also observed in non-ImP-labeled processes (arrowheads), such as the AT_1-ImG labeling of a glial process (d) and a presynaptic terminal (a), and the p47-ImG labeling of a myelinated axon (h), and gial processes (e, h). Scale bars: 0.5 μm.

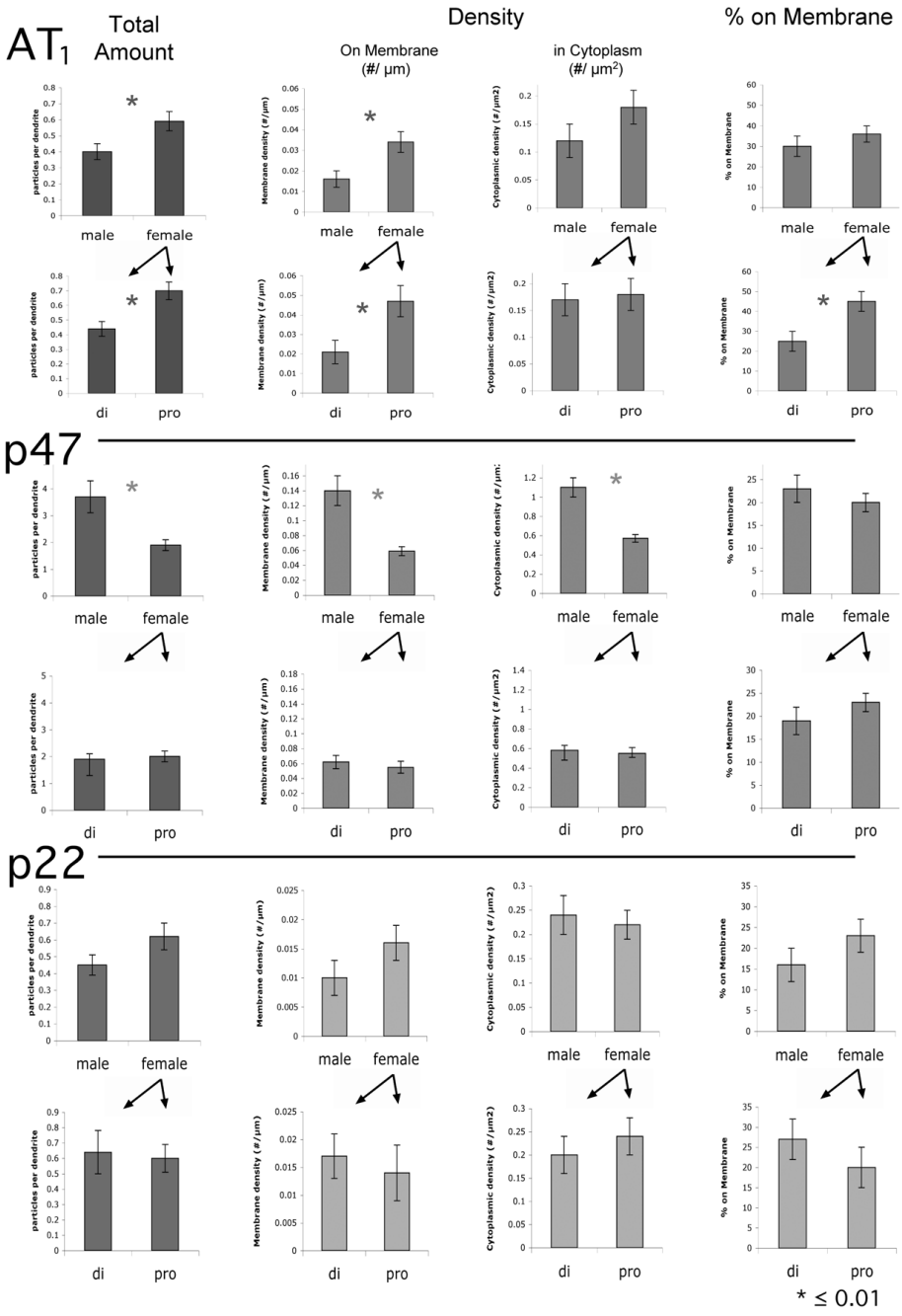

Fig. 4.

Histograms of the average total number of ImG particles observed per ImP-labeled profile (Total Amount), the average density of ImG particles on the profile membrane (#/µm) and in the cytoplasm of the profile (#/µm^2), and the average percentage of ImG particles on the profile membrane (versus in the cytoplasm), for AT_1, p47 and p22-ImG particles. Sets of histograms (containing male/female values, and di (diestus)/pro (proestrus) values) are horizontally arranged by antibody, and vertically arranged by measure. * ≤ 0.01.